

Regulation of structural and functional synapse density by L-threonate through modulation of intraneuronal magnesium concentration



Qifeng Sun ^a, Jason G. Weinger ^b, Fei Mao ^b, Guosong Liu ^{a, b, *}

^a School of Medicine, Tsinghua University, Beijing, 100084, China

^b Neurocentria, Inc., Fremont, CA 94538, USA

ARTICLE INFO

Article history:

Received 30 November 2015

Received in revised form

18 April 2016

Accepted 9 May 2016

Available online 10 May 2016

Keywords:

Threonate

Synaptic density

Functional terminals

Intracellular Mg²⁺

Rat

Human stem cell-derived neurons

ABSTRACT

Oral administration of the combination of L-threonate (threonate) and magnesium (Mg²⁺) in the form of L-Threonic acid Magnesium salt (L-TAMS) can enhance learning and memory in young rats and prevent memory decline in aging rats and in Alzheimer's disease model mice. Recent results from a human clinical trial demonstrate the efficacy of L-TAMS in restoring global cognitive abilities of older adults. Previously, we reported that neuronal intracellular Mg²⁺ serves as a critical signaling molecule for controlling synapse density, a key factor that determines cognitive ability. The elevation of brain Mg²⁺ by oral administration of L-TAMS in intact animals plays a significant role in mediating the therapeutic effects of L-TAMS. The current study sought to elucidate the unique role of threonate. We aimed to understand if threonate acts directly to elevate intraneuronal Mg²⁺, and why Mg²⁺ given without threonate is ineffective for enhancing learning and memory ability. We discovered that threonate is naturally present in cerebrospinal fluid (CSF) and oral treatment with L-TAMS elevated CSF threonate. In cultured hippocampal neurons, threonate treatment directly induced an increase in intracellular Mg²⁺ concentration. Functionally, elevating threonate upregulated expression of NR2B-containing NMDAR, boosted mitochondrial membrane potential ($\Delta\Psi_m$), and increased functional synapse density in neuronal cultures. These effects are unique to threonate, as other common Mg²⁺ anions failed to have the same results. Mechanistically, threonate's effects were specifically mediated through glucose transporters (GLUTs). We also evaluated the effects of threonate in human neural stem cell-derived neurons, and found it was equally effective at upregulating synapse density. The current study provides an explanation for why threonate is an essential component of L-TAMS and supports the use of L-TAMS to promote cognitive abilities in human.

© 2016 The Authors. Published by Elsevier Ltd. This is an open access article under the CC BY license (<http://creativecommons.org/licenses/by/4.0/>).

1. Introduction

L-Threonate, (2R,3S)-2,3,4-Trihydroxybutanoate, is a naturally occurring sugar acid present in the body, with the structure C₄H₇O₅. It has been found in the periphery in plasma and the aqueous humor of the eye (Deutsch et al., 1999; Harding et al., 1999). How threonate is eliminated from the body is not fully understood; however, so far we know that approximately 10% is excreted in urine (Lawson et al., 1976; Thompson et al., 1975; Wang et al., 2011).

Recent studies show that threonate might have a physiological function. In the periphery, threonate has been linked to bone health. Threonate can prevent bone degradation by inhibiting

osteoclast resorption from bone (He et al., 2005). Threonate also supports bone formation in two ways. One, it promotes calcium bioavailability, allowing for rapid absorption of calcium into the body (Wang et al., 2013). Two, threonate increases bone mineralization by inhibiting DHT-inducible dickkopf-1 (DKK-1) expression. DKK-1 is an osteoblast inhibitory factor whose overexpression can negatively impact bone formation and density (Kwack et al., 2008, 2010; Monroe et al., 2012).

Our previous work showed that threonate also has effects in the central nervous system (CNS). Oral treatment with the combination of threonate and magnesium (Mg²⁺) in the form of L-threonic acid Magnesium salt (L-TAMS) increases synapse density and memory ability in both aged rats and late stage Alzheimer's disease (AD) model mice (Li et al., 2014; Slutsky et al., 2010). A recent study shows that L-TAMS is also effective at improving cognitive deficits in humans (Liu et al., 2015).

* Corresponding author. Neurocentria, Inc., Fremont, CA 94538, USA.
E-mail address: gliu@neurocentria.com (G. Liu).

Cognitive decline is best correlated with brain atrophy associated with synaptic loss (Jack et al., 2015; Ridha et al., 2006; Terry et al., 1991). In fact, alteration of synaptic efficacy in the hippocampus is an initial event in cognitive disorders such as AD (Selkoe, 2002). Considering synapses are the elemental unit of neural computation, it is not surprising that the both the physical loss of synapses (reduced structural density) and the loss of function among the remaining synapses (reduced functional synapse density) are associated with impaired cognition. Notably, we have demonstrated that neuronal intracellular Mg^{2+} concentration [Mg^{2+}] is a critical signaling molecule regulating structural and functional terminal density, with higher intracellular [Mg^{2+}] resulting in greater structural and functional terminal density (Zhou and Liu, 2015).

Our work has shown that not only does neuronal intracellular Mg^{2+} promote structural synapse density and plasticity, but it also controls whether presynaptic terminals are functional or nonfunctional (Zhou and Liu, 2015). Functional synapses are able to release neurotransmitter containing vesicles and thus affect the post-synaptic neuron, while nonfunctional synapses are structurally present but fail to release neurotransmitter and are unable to signal to the post-synaptic neuron.

Threonate is a critical component of L-TAMS; when animals are treated with Mg^{2+} that is not coupled to threonate (ie. an alternate anion such as chloride is used), there is no significant effect on memory ability (Slutsky et al., 2010). However, threonate treatment alone, without Mg^{2+} , also does not affect memory ability, suggesting that there is a synergistic effect between threonate and Mg^{2+} (Slutsky et al., 2010).

While L-TAMS has been shown to be effective at improving cognition, there are still unanswered questions about the unique role of threonate and why L-TAMS treatment is effective at improving learning and memory ability but Mg^{2+} treatment in the absence of threonate is not. These questions were examined in the current study. Specifically, we investigated if there is uptake of threonate into the CNS following oral treatment with L-TAMS, and if threonate itself has any effects on hippocampal neurons. Because threonate and Mg^{2+} are both required for effects on cognition in an intact animal, we explored their interaction, focusing on how threonate affects Mg^{2+} homeostasis in the neuron, and functional/structural synapse density. Finally, and perhaps most importantly, we asked whether threonate is naturally present in the CNS and if it has any physiological functions.

2. Materials and methods

2.1. Experimental animals

Male Sprague-Dawley rats were purchased from Vital River Laboratory (Animal Technology Co. Ltd., Beijing, China) and bred in Tsinghua University's laboratory animal center. All rats were individually housed in a controlled environment, under an inverted light cycle (light onset at 8:00 p.m. to 8:00 a.m.) and had free access to food and water. On arrival and before the start of the experiments (see below), rats were fed a commercial pelleted diet (Shanghai SLAC Laboratory Animal Co. Ltd), containing normal Mg^{2+} (0.15%) and tap water ad lib. All procedures on rats were approved by Tsinghua University Committee on Animal Care.

2.2. Threonate measurement in plasma and CSF

For testing baseline plasma and CSF threonate concentrations, 3 month old rats were fed deionized water without threonate for 1 month. Water was removed for 6 h prior to sample collection as a washout period. Then, using the previously describe minimum

effective dose of L-TAMS (Neurocentria, Inc., CA, USA) in rats (604 mg/kg/day) (Slutsky et al., 2010), rats were administered either L-TAMS (via deionized drinking water) for 1 month or water only (control). Rat chow for both groups contained basic nutritional Mg^{2+} concentration at 0.15%. Prior to blood and CSF collection, water was removed for 6 h as a washout period.

To determine threonate concentrations in the plasma and cerebrospinal fluid (CSF), rats were anesthetized with Chloral hydrate (350 mg/kg, i.p.), and then blood and CSF samples were collected from the orbital sinus and cisterna magna, respectively. Blood (0.5–1 ml/rat) and CSF (50–100 μ L/rat) samples were collected, centrifuged, and stored at -20°C until threonate measurement was performed.

Threonate levels in plasma and CSF were determined by high-performance liquid chromatography-tandem mass spectrometry (HPLC-MS/MS, Center of Biomedical Analysis, Tsinghua University) as described previously (Wang et al., 2006). Briefly, after a simple protein precipitation with methanol, Plasma and CSF samples were centrifuged at 14,800 rpm for 15 min, and then the supernatants were collected for analysis. An Eclipse Plus C18 column (4.6 \times 100 mm, 3.5 μ m) (Agilent Technologies, Santa Clara, CA, USA) was employed to separate the analyte. The mobile phase consisted of two solvents: 12.5 mM ammonia, 15 mM ammonium acetate in water (A) and 100% methanol (B). Gradient conditions: 0–2.5 min 90% A/10% B; 2.5–5 min 90–20% A/10–80% B. The flow rate was 0.4 μ L/min. The Agilent 6460 triple Quadrupole mass spectrometer, equipped with Electrospray Ion Source (EIS) was operated under a negative ionization mode. Multiple reactions monitoring (MRM) transition of m/z 135.1 \rightarrow 75.0 was chosen to quantify threonate. Calibration curves were obtained for the following range of threonate concentrations: 10–1000 nM/L.

2.3. Hippocampal neuron cultures

Hippocampal neurons were prepared from postnatal d1 rats from Vital River Laboratory and cultured as previously described (Liu et al., 1999; Liu and Tsien, 1995). Following a previously described neuronal culture protocol (Kaech and Banker, 2006), and based on the known insulin/insulin-like growth factor concentrations in rat (Steffens et al., 1988), we added 10 ng/ml insulin (in addition to insulin in B27) into 0.6 mM extracellular [Mg^{2+}] culture medium. 2 days after plating, cytosine arabinoside (ARA-C, Sigma) was added to a final concentration of 2.5 μ M to inhibit glial proliferation. Neurons were plated onto Matrigel (BD)-coated 8 \times 8 mm coverslips or 6-well plates (Corning).

2.4. Treatment with threonate and other anions

We used sodium-L-threonate (NaT, Biotium, USA) to study short-term (4 h) and long-term (2 days) treatment of threonate on mature hippocampal neurons (14–21 days *in vitro*: DIV). The following anions were used in this study: citrate (200 μ M), gluconate (1 mM), malate (5 μ M) and glycinate (400 μ M) (all from Sigma). The dosage of analogs in culture medium was determined by their known concentrations *in vivo* (Hoffmann et al., 1993; Subramanian et al., 2005). For chemical structures see Supplemental Fig. 1.

2.5. Intracellular free Mg^{2+} analysis

Intracellular [Mg^{2+}] was determined by using Magnesium Green™ (MgGreen, Invitrogen) as described previously (Fox et al., 2007; Zhou and Liu, 2015). Briefly, neurons were incubated in 2 ml tyrode's buffer (NaCl, 124 mM; KCl, 5 mM; CaCl_2 , 2 mM; MgCl_2 , 1 mM; glucose, 30 mM; and HEPES, 25 mM, pH 7.4 with NaOH)

with 5 μg MgGreen dissolved for 30 min at 37 °C, then washed 3 times, and images were collected using an Olympus IX-70 confocal microscope with a 60 \times water lens, at a 4 \times zoom. As described by Zhou and Liu (Zhou and Liu, 2015):

$$[\text{Mg}^{2+}]_i \propto \frac{F_{(a.u.)}}{D_{\text{diameter}}}$$

Where $F_{(a.u.)}$ is the mean fluorescent density (arbitrary units) in the branch of interest which was quantified using Image-Pro Plus software (IPP, Media Cybernetics, Carlsbad, CA), and D_{diameter} is the mean width of the same selected branch in differential interference contrast (DIC) image.

2.6. Calculation of functional terminal density by FM1-43 imaging

The technique to quantify a functional terminal is detailed in Zhou and Liu (Zhou and Liu, 2015). Functional terminal density at a dendritic branch was defined as the number of synaptic terminals that can undergo synaptic vesicle turnover after physiological stimulation per unit area of dendritic branch. We used FM-dye staining to determine the functional status of a synaptic terminal. Briefly, mature hippocampal neurons (14–21 DIV) were stained with 10 μM FM1-43 (synaptogreen, Biotium) following physiological pattern of stimulus (6 bursts of 5 APs each at 100 Hz with a 10 s interburst interval) to get image F_1 , as described by (Slutsky et al., 2004; Zhou and Liu, 2015). Background was determined by the image following destaining (480 APs at 2 Hz; F_2). ΔF ($\Delta F = F_1 - F_2$) is proportional to the number of vesicles undergoing endocytosis after physiological stimuli. A terminal is considered to be functional if it can release at least one vesicle after 30 APs staining stimulation.

Fluorescent images were acquired with an Olympus IX-70 confocal microscope with a 60 \times water lens (numerical aperture; NA = 1.2) at a dimension of 78.6 \times 78.6 μm . The density of functional terminal was estimated by using IPP. Each ΔF image was the F_1 loading image minus the F_2 unloading image ($\Delta F = F_1 - F_2$). The number of FM1-43+ puncta (N) was measured from the corresponding ΔF image. The length (l), diameter (d), and calculated area ($A = l \times d$) of each branch was determined from DIC images. The number of FM1-43+ puncta per μm^2 of dendrite (N/A) was calculated to determine the density of functional terminal in the branch, and the mean density of 30–50 branches was averaged to represent the functional terminal density in one ΔF image. We obtained image of ΔF from loading image F_1 and unloading image F_2 ($\Delta F = F_1 - F_2$).

2.7. Measurement of mitochondrial function

Mitochondrial function of hippocampal neurons was observed microscopically (Olympus IX-70) by using 5,5',6,6'-tetrachloro-1,1',3,3'-tetraethylbenzimidazolyl-carbocyanine iodide (JC-1, Invitrogen) (Smiley et al., 1991; Szelechowski et al., 2014). The monomeric form of JC-1 has an emission maximum at 529 nm. At higher concentrations or potentials the dye forms red fluorescent J-aggregates with an emission maximum of 590 nm. The ratio of J-aggregate/J-monomer is used as an estimate of transmembrane potential ($\Delta\Psi_m$).

Mature neurons were loaded for 20 min at 37 °C with 1 μM JC-1 in tyrode's buffer. After loading, neurons were washed twice with tyrode's buffer, and 3–5 images were collected from the coverslip at $\times 180$ magnification. Each sequential JC-1 monomer (green; 510–575 nm) and JC-1 aggregate (red; >575 nm) image was collected at the same time. Then we calculated the ratio of fluorescence at >575 nm (red) versus 510–575 nm (green) ($F_{\text{aggregate}}/F_{\text{monomer}}$) to represent the $\Delta\Psi_m$ of each individual mitochondrion.

$\Delta\Psi_m > 0.26$ ($F_{\text{aggregate}}/F_{\text{monomer}}$) was set as the lower threshold, as defined previously (see method in (Zhou and Liu, 2015)). The average $\Delta\Psi_m$ of all mitochondrial puncta in 3–5 images represents the average $\Delta\Psi_m$ of a coverslip, and the mean $\Delta\Psi_m$ of 5–8 coverslips represents the mean $\Delta\Psi_m$ of each group. The number of JC-1 aggregate(+) fluorescent puncta represents the number of mitochondrion, since the number of mitochondrion by measuring number of JC-1 aggregate(+) fluorescent puncta was the same as measuring number of Mito-View633(+) puncta (Zhou and Liu, 2015). DIC images were used to measure the area of each branch. N_{MITO} was calculated to represent the level of mitochondrial density (number of mitochondrion per area of branches). $N_{\text{MITO}} \times \Delta\Psi_m$ was generated to show the functional status of mitochondrion.

2.8. Differentiation of human neural stem cells to neurons

Human fetal cortices-derived neural stem cells (hNSC; Angecon, China) were cultured in hNSC medium (Angecon) according to guidelines provided by Angecon. hNSCs were maintained in this medium for 10–14 days, passaged using Accutase (Invitrogen), washed and replated at a dilution of 1:3 to 1:5.

We used a previously described differentiation protocol to differentiate hNSCs to neurons (Shi and Jiao, 2012). Briefly, hNSC cultures were dissociated into single cells with Accutase, and then plated on polyornithine/laminin (Sigma)-coated 6-well plates at 50,000 cells per cm^2 in neural maintenance medium with EGF (Invitrogen) and FGF2 (Pepro Tech) at a concentration of 10 ng ml^{-1} . Neural maintenance medium consists of a 1:1 mixture of DMEM/F12 and Neurobasal medium (Invitrogen), 1 \times N2 (Invitrogen), 1 \times B27 (Invitrogen), 1 mM L-glutamine, 0.1 mM non-essential amino acids, 5 $\mu\text{g ml}^{-1}$ insulin, 0.1 mM 2-mercaptoethanol, 25 U ml^{-1} penicillin and 25 mg ml^{-1} streptomycin. After 3–4 days, when cells reached 95% confluency, culture medium was changed to a neural induction medium, consisting of neural maintenance medium, 500 ng ml^{-1} Noggin (R&D Systems) and 10 μM SB431542 (Tocris). Neurons were maintained 10–14 days in this medium; medium was replaced every day. When neuroepithelial cells appeared, Dispase (Roche) was used to collect cells. They were replated in neural maintenance medium with EGF and FGF2 at 20 ng ml^{-1} for 2–4 days, then changed to neural maintenance medium and cultured for up to 80 days, replacing medium every other day.

2.9. Immunocytochemistry

Neuronal cultures were washed three times in 0.01 M PBS followed by fixation for 20 min in 4% paraformaldehyde at 4 °C. The neuronal culture coverslips were then washed in 1 \times PBS before incubation in blocking solution containing 0.1% Triton X-100 and 1% bovine serum albumin for 30 min at room temperature. Then, neurons were incubated with mouse anti-PSD-95 (AB2723, Abcam, 1:100), guinea pig anti-MAP2 (188004, Synaptic Systems, 1:300) and rabbit anti-synaptophysin (MAB5258, Millipore, 1:100) in blocking solution at 4 °C overnight. On the following day, neurons were rinsed with 1 \times PBS before 2 h incubation with secondary antibodies including: donkey anti-mouse IgG-CF 488A 1:100, donkey anti-guinea pig IgG-CF 555 1:300 and donkey anti-rabbit IgG-CF 640R 1:200 (Biotium). Finally, neurons were mounted onto slides with anti-fade fluorescent mounting medium (Vector Laboratories) and stored at 4 °C for 2 days.

2.10. Quantification of Synaptophysin and PSD-95

Cultures were imaged with a confocal laser inverted microscope (Olympus IX-70) equipped with a 60 \times (NA 1.2) objective. Each

image was collected at a 4× zoom at a resolution of 1024 × 1024 with a serial z projection of 5 images (thickness of 0.8 μm). Then, the stack of images was compressed to generate a final image at the maximal intensity. Synaptophysin (Syn) staining (red puncta) and PSD-95 staining (green puncta) were aligned to generate Co-localized Syn & PSD-95 staining (yellow puncta) images.

The density of Syn, PSD-95, and Co-localized Syn & PSD-95 + puncta was estimated by using IPP. We equalized background levels and separated fluorescent puncta with IPP filters. 50–60 branches were selected from a MAP2 stained image, the length (l) and diameter (d) of each branch were measured, and $l \times d$ was calculated to estimate the area (A) of the branch. The number of red, green, and yellow puncta (N) was measured from the same branch. N/A was calculated separately for red, green, and yellow puncta, which represented the density of puncta in the branch. The mean density of the 50–60 branches was calculated to estimate the density of Syn, PSD-95, and Co-localized Syn & PSD-95 + puncta in one image, and the values from 5 to 7 images were averaged to determine the mean puncta density in a coverslip.

2.11. Western blot

Samples of threonate-treated and control hippocampal neurons were solubilized in RIPA buffer (Sigma) containing protease inhibitors (Roche) and phosphatase inhibitors (Roche), and then equal amount of proteins were loaded onto 10% polyacrylamide gels. Proteins were transferred to PVDF membranes (Millipore), and probed with primary antibodies including Synaptophysin (Millipore), RIM1, Rab3a (both from Synaptic System), PSD-95, NR2B, β -tubulin and β -actin (all from Cell Signaling Technology), followed by an appropriate HRP-coupled secondary antibody (Cell Signaling Technology). The signals were detected by ECL detection reagent (GE Healthcare) and captured on autoradiography film (Kodak). For quantification of protein signals, the integrated optical density (IOD) was measured with IPP, and β -tubulin or β -actin in the same lane served as a loading control.

2.12. Transfection

Green fluorescent protein (GFP)-expressing NR2B (GFP-NR2B) (Luo et al., 2002) and mKate2 (Shcheglovitov et al., 2013) plasmids (mKate2 was used as a transfection control) were co-transfected into 7 DIV neurons plated on coverslips, using the Ca^{2+} phosphate method. The transfection medium was prepared with DMEM (Gibco) and DNA- Ca^{2+} -phosphate precipitate was prepared using Clontech CalPhos Mammalian Transfection Kit (BD Bioscience). After transfection, on 14 DIV, half of the coverslips were treated with 150 μM threonate for 2 days before imaging. Images were collected at a resolution of 512 × 512 with a pixel width of 0.267 μm using a CCD camera (Andor). A 60× NA 1.20 water-immersion objective (Olympus) was used. Z-stacks of GFP-NR2B and mKate2 were photographed with 0.5 μm step, and then projected at maximum in the z direction. For each spine, the fluorescence of GFP-NR2B and mKate2 was measured in the open-source software Fiji (ImageJ) and the ratio ($F_{\text{GFP-NR2B}}/F_{\text{mKate2}}$) was used to represent the quantity of expression of NR2B, where F_{mKate2} was used to calibrate the efficiency of transfection and the local volume of the spine.

2.13. Statistical analysis

All data are shown as mean ± SEM (standard error of the mean). Statistical significance was determined by two-tailed paired (same rats)/unpaired Student's t test, Kolmogorov–Smirnov test, or one-way/two-way ANOVA, followed by Bonferroni's post hoc test. N

represents total number of rats, and n represents the total number of separate cultures or coverslips. $P < 0.05$ was considered statistically significant.

3. Results

3.1. Body distribution of threonate and accumulation of threonate in CSF after oral threonate treatment

Initially, we examined the distribution of threonate in the body. Similar to previous reports (Wang et al., 2006, 2013), plasma threonate concentration was approximately 20 μM. Interestingly, in the CSF, threonate concentration was approximately 100 μM, about 5-fold higher than in the periphery ($p < 0.001$, Fig. 1A). Then, we studied the effects of oral dosing of L-TAMS (604 mg/kg/day) on the plasma and CSF concentrations of threonate. Since it takes >2 weeks of L-TAMS treatment to have a noticeable effect on CSF Mg^{2+} concentration and memory function, we monitored the concentration of threonate in plasma and CSF after 1 month treatment (Slutsky et al., 2010) (see experimental paradigm, Fig. 1). Following oral L-TAMS treatment for 1 month, and 6 h washout, threonate concentration did not change in plasma (Fig. 1B), indicating there was no accumulation in the periphery and that it could be quickly cleared (within 6 h). In contrast, threonate concentration increased significantly in the CSF by 54% ($p = 0.01$, Fig. 1C). These data indicate that with L-TAMS treatment, threonate accumulated in the CNS compartment, leading to sustained elevation of brain threonate, while in the peripheral compartment threonate did not accumulate.

3.2. Raising extracellular threonate concentration promotes elevation of intracellular magnesium concentration

Our recent studies indicate that synaptic changes after raising extracellular $[\text{Mg}^{2+}]$ are due to an increase of intracellular $[\text{Mg}^{2+}]$ (Zhou and Liu, 2015). Therefore, we asked whether treatment with threonate would elevate intracellular $[\text{Mg}^{2+}]$ in cultured rat hippocampal neurons. Since we were interested in the effects of threonate on neuronal function, and hypothesized that any effects are mediated through changes in intracellular magnesium concentration, we tested the effects of threonate over a range of extracellular $[\text{Mg}^{2+}]$, including 0.6, 0.8 and 1.2 mM. Since 0.8 mM extracellular $[\text{Mg}^{2+}]$ in brain is considered physiological and there are reports of age-dependent and pathophysiological-related reductions (such as in Alzheimer's Disease) in CSF magnesium of 20–30%, 0.6 mM extracellular $[\text{Mg}^{2+}]$ represented this observed lower Mg^{2+} concentration (Andrasi et al., 2005; Cillier et al., 2007). Neurons were cultured for two weeks at 0.6, 0.8, or 1.2 mM extracellular $[\text{Mg}^{2+}]$. Intracellular $[\text{Mg}^{2+}]$ was quantified by MgGrn fluorescent dye (see methods). Intracellular $[\text{Mg}^{2+}]$ was significantly higher at 0.8 and 1.2 mM extracellular $[\text{Mg}^{2+}]$ than at 0.6 mM extracellular $[\text{Mg}^{2+}]$ ($F_{2,19} = 39.10$, $p < 0.0001$; Fig. 2A, B). These observations are consistent with our previous finding that extracellular $[\text{Mg}^{2+}]$ affected intracellular $[\text{Mg}^{2+}]$ with a bell-shaped relationship (Zhou and Liu, 2015). 2 day treatment with threonate (0–200 μM) induced an increase of intracellular $[\text{Mg}^{2+}]$ in a dosage-dependent manner at various extracellular $[\text{Mg}^{2+}]$ (0.6 mM Mg, $F_{4,26} = 19.03$, $p < 0.0001$; 0.8 mM Mg, $F_{4,27} = 12.88$, $p < 0.0001$; 1.2 mM Mg, $F_{4,25} = 17.78$, $p < 0.0001$; Fig. 2A, B), up to 150 μM threonate (Fig. 2B). Using the threonate concentration that induced the largest change in intracellular $[\text{Mg}^{2+}]$ (150 μM), we performed a time course analysis of the effects of threonate on intracellular $[\text{Mg}^{2+}]$ (Fig. 2C, D). Threonate effects were maximal at 2 h and this increase persisted for the entire course of the experiment ($F_{5,26} = 10.83$, $p < 0.0001$; Fig. 2D). Intracellular $[\text{Mg}^{2+}]$

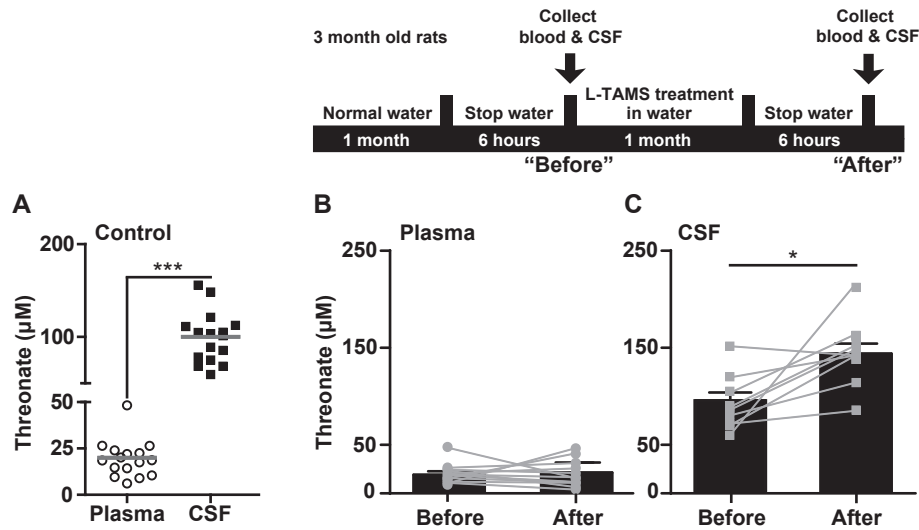


Fig. 1. Elevation of brain threonate by L-TAMS. (A) Threonate concentrations (μM) in plasma and CSF were determined in 4 month old rats ($N = 16$) fed with normal chow and water. Each circle or square represents an individual rat. (B–C) Schematic of L-TAMS treatment paradigm. 3 month old rats were treated with normal water for one month, then blood and CSF were collected after a 6 h washout period ("Before"), which constituted the control samples. Then rats were treated for one month with L-TAMS and blood and CSF samples were collected after a 6 h washout period ("After"). Threonate concentrations (μM) in the plasma (B; $N = 12$) and CSF (C; $N = 9$) were determined before and after 1 month treatment with L-TAMS. The concentration in plasma and CSF for each timepoint is shown for each rat. The average of each group at each timepoint is shown in the histogram behind the individual rat data. Unpaired t test (A), paired t test (B, C); * $p < 0.05$, *** $p < 0.001$.

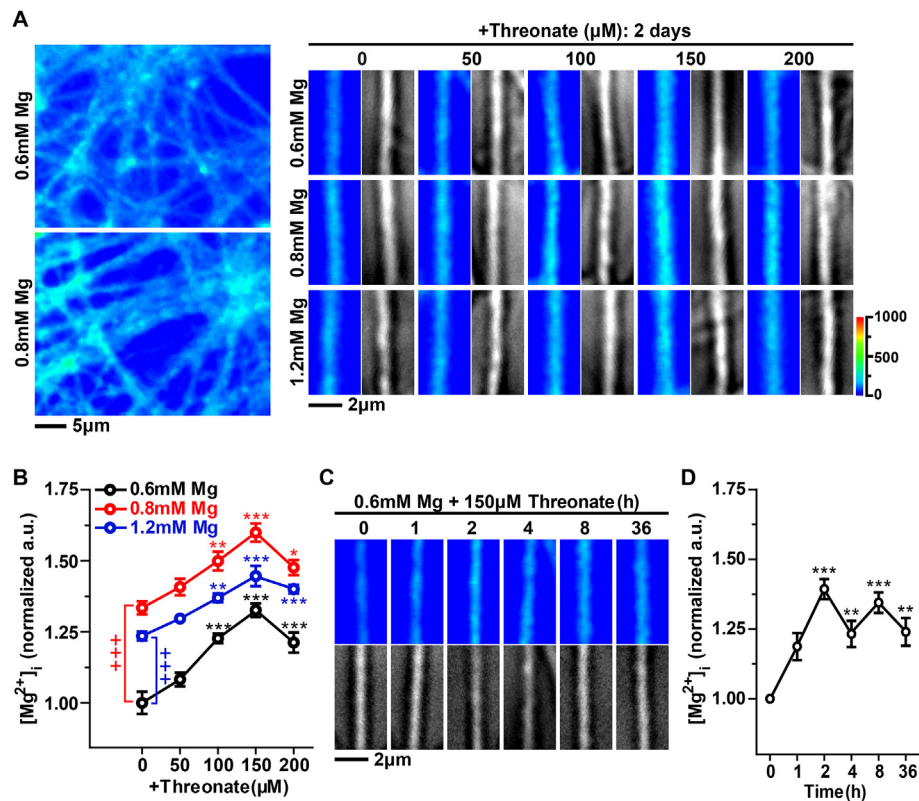


Fig. 2. Raising extracellular threonate concentration promotes elevation of intracellular Mg^{2+} concentration ($[\text{Mg}^{2+}]_i$). (A) Left panel) Representative MgGreen fluorescent images (pseudo-colored) of dendrites with extracellular Mg^{2+} concentration ($[\text{Mg}^{2+}]_o$) of 0.6 mM and 0.8 mM. Right panel) High magnification images of MgGreen (pseudo-colored images) and DIC (gray), showing individual branches with varying concentrations of $[\text{Mg}^{2+}]_o$ (0.6 or 0.8 or 1.2 mM Mg; long-term, LT = 2 weeks) and threonate (0–200 μM ; 2 days). (B) $[\text{Mg}^{2+}]_i$ was calculated as normalized $F_{(a,u)}$ by dividing each branch's MgGreen $F_{(a,u)}$ by its mean diameter (measured from DIC images). The resulting averages for each $[\text{Mg}^{2+}]_o$ and threonate concentration are displayed. One-way ANOVA compared differences in $[\text{Mg}^{2+}]_i$ at different $[\text{Mg}^{2+}]_o$ (0.6 mM Mg, $n = 7$; 0.8 mM Mg, $n = 8$; 1.2 mM Mg, $n = 7$ coverslips). For each $[\text{Mg}^{2+}]_o$, one-way ANOVA compared neuronal $[\text{Mg}^{2+}]_i$ in response to increasing threonate concentrations ($n = 5$ –6 per concentration) relative to 0 μM threonate (control); +++ $p < 0.001$; * $p < 0.05$; ** $p < 0.01$; *** $p < 0.001$. (C) Representative MgGreen (pseudo-colored) and DIC (gray) fluorescent images of individual branches after time course (0–36 h) of threonate treatment (150 μM). (D) Time course line graph of average neuronal $[\text{Mg}^{2+}]_i$ ($n = 4$ –6); one-way ANOVA and Bonferroni's post hoc test, ** $p < 0.01$, *** $p < 0.001$ versus control (h 0).

following long-term treatment (>2 weeks) of threonate was similar to short-term threonate treatment (data not shown).

3.3. Raising extracellular threonate concentration increases synaptic density and upregulates NR2B-containing NMDAR expression

Our previous study shows that intracellular $[Mg^{2+}]$ plays an important role in controlling structural and functional synapse density. Since threonate treatment elevated intracellular $[Mg^{2+}]$, it is of interest to determine if elevation of threonate can also increase synaptic density and plasticity.

Presynaptic terminal density was quantified by the density of Synaptophysin (Syn) puncta (number per μm^2) (Lowenstein et al., 1995; Tarsa and Goda, 2002) and postsynaptic glutamatergic synapse density was quantified by the density of PSD-95 puncta (Hunt et al., 1996). Overall synapse density was determined by the colocalization of Syn and PSD-95 expression (Glantz et al., 2007; Siew et al., 2004). Threonate treatment significantly upregulated the number of Syn puncta, PSD-95 puncta (Syn, $F_{3,16} = 4.318$, $p = 0.0207$; PSD-95, $F_{3,16} = 6.315$, $p = 0.005$; Fig. 3A, B: left panel), and Syn/PSD-95 co-localized puncta (Co-localization, $F_{3,16} = 5.653$, $p = 0.0078$; Fig. 3A, B: middle panel). We also checked whether threonate changed the percentage of excitatory synapses, which is defined as the number of Syn/PSD-95 co-localized puncta divided by the number of Syn puncta. With threonate treatment, the percentage of excitatory synapses did not significantly change (Fig. 3A, B: right panel), suggesting that threonate treatment did not change the balance of the neuronal network.

We used Western blot to verify the increase of pre- and post-synaptic proteins in hippocampal neuronal cultures following threonate treatment. After 2 days of threonate treatment, Syn and PSD-95 expression were significantly increased (Fig. 3C). We also checked the expression of two presynaptic proteins critical for the functional status of presynaptic terminals, Rab3a and RIM1 (Zhou and Liu, 2015). Similar to Syn and PSD-95, Rab3a and RIM1 expression were significantly increased following threonate treatment (Syn: $F_{3,44} = 7.38$, $p = 0.0004$, $n = 12$; PSD-95: $F_{3,36} = 3.350$, $p = 0.0295$, $n = 10$; Rab3a: $F_{3,56} = 12.45$, $p < 0.0001$, $n = 15$; RIM1: $F_{3,24} = 5.946$, $p = 0.0035$, $n = 7$; Fig. 3C).

NR2B-containing NMDAR plays an important role in controlling synaptic plasticity (Le Roux et al., 2007). Upregulation of its expression is sufficient to enhance learning and memory ability (Tang et al., 1999). Elevation of extracellular $[Mg^{2+}]$ can selectively increase synaptic NR2B-containing NMDAR (Slutsky et al., 2004, 2010). We checked whether threonate treatment can also affect NR2B. Threonate treatment significantly upregulated NR2B-containing NMDAR in hippocampal neurons ($F_{3,17} = 7.493$, $p = 0.0021$; Fig. 4A).

To assess whether threonate treatment increased synaptic NR2B expression, we transfected neurons with GFP-labeled NR2B (GFP-NR2B), using mKate2 transfection as an internal control. $F_{GFP-NR2B}/F_{mKate2}$ in each individual spine represents the expression of NR2B. Threonate treatment directly elevated expression of synaptic NR2B. On average, $F_{GFP-NR2B}/F_{mKate2}$ was 30% higher in threonate group (Kolmogorov-Smirnov test, $p < 0.0001$; Fig. 4B, C).

Collectively, threonate-treated neurons exhibited higher structural synaptic density, and higher expression of proteins critical for synaptic plasticity.

3.4. Threonate increases functional presynaptic terminal density and enhances mitochondrial function

Having studied the effects of threonate on structural synaptic density, we next investigated the effects of threonate on

presynaptic terminal function. We used FM dye to evaluate the terminals' ability to undergo activity dependent vesicular turnover (Liu and Tsien, 1995; Ryan et al., 1993; Slutsky et al., 2004). Vesicular endocytosis triggered by stimulation results in FM dye uptake. Terminals labeled by FM as a result of physiological pattern of stimulus are defined as functional (for detailed experimental protocol see (Zhou and Liu, 2015)). Mature hippocampal neuronal cultures (14–21 DIV) with varying concentrations of extracellular $[Mg^{2+}]$ (0.6, 0.8, 1.2 mM) were treated with threonate (0–150 μM) for 2 days. The FM dye staining results are shown in Fig. 5A. Threonate treatment induced a similar pattern of change in functional terminal density as it did in intracellular $[Mg^{2+}]$ (Fig. 2B). The number of functional terminals was significantly higher at 0.8 and 1.2 mM than 0.6 mM extracellular $[Mg^{2+}]$ ($F_{2,14} = 14.27$, $p = 0.0004$; Fig. 5A, B), and increased following threonate treatment in a dose-dependent manner under all extracellular $[Mg^{2+}]$ conditions tested (0.6 mM Mg: $F_{3,21} = 15.15$, $p < 0.0001$; 0.8 mM Mg: $F_{3,16} = 8.946$, $p = 0.001$; 1.2 mM Mg: $F_{3,16} = 3.088$, $p = 0.057$; Fig. 5A, B).

Next, we evaluated the effects of threonate treatment on the release probability (Pr) of individual synapses and the total synaptic input per unit area of dendrite to determine whether the increase of functional synapse density affects the homeostasis of synaptic input to the dendrite (Liu and Tsien, 1995). We used a 30 APs at 0.5 Hz stimulation protocol to determine the Pr of a single terminal, described previously (Slutsky et al., 2004). Interestingly, while threonate treatment lead to an ~27% increase in terminal density (N), it also induced the reduction of Pr by ~20%, such that total synapse inputs (S) to a unit area of dendrite remained constant (Fig. 5 C, D), indicating that the homeostasis of functional synapse density and individual synapse Pr remains constant during threonate treatment.

Our recent data show that the local energy supply critically determines the functionality of terminals. Intracellular $[Mg^{2+}]$ plays a pivotal role in controlling mitochondrial efficiency, which in turn determines the local energy supply and functional terminal density. If threonate can elevate intracellular $[Mg^{2+}]$, it might improve the functional status of mitochondria, leading to an increase in functional terminal density. To assess mitochondrial function, we examined their density (N_{MITO}) and membrane potential ($\Delta\Psi_m$) in the network, two important parameters for quantification of mitochondria function ($N_{MITO} \times \Delta\Psi_m$) (Buckman and Reynolds, 2001; Nicholls and Ward, 2000). We used the ratio of J-aggregate to J-monomer form of JC-1 to estimate $\Delta\Psi_m$ (see methods) (Smiley et al., 1991; Szelechowski et al., 2014). Addition of threonate for 2 days to hippocampal neurons significantly increased N_{MITO} by 9.2%, enhanced $\Delta\Psi_m$ by 49.6%, and improved ($N_{MITO} \times \Delta\Psi_m$) by 63% compared to controls (Unpaired t test, $p < 0.01$; Fig. 5E, F), suggesting that threonate treatment enhanced neuronal mitochondrial function.

3.5. Comparison of effects of various anions on intracellular magnesium and functional synaptic density

The above data suggests that threonate has a direct effect in promoting an increase of intracellular $[Mg^{2+}]$. For elevation of hippocampal neuron $[Mg^{2+}]$, it was of interest to see whether other major anions have a similar effect. By comparing the molecular structure of compounds that have or do not have this effect, one might be able to ascertain the membrane channel/carrier involved in elevation of intracellular $[Mg^{2+}]$.

For comparison, we selected malate, citrate, and gluconate for their structural similarity to threonate as sugar acids, and glycinate because it is purported to promote cation absorption in the periphery (Hertrampf and Olivares, 2004). These molecules were tested under 0.6 mM extracellular $[Mg^{2+}]$ conditions, and

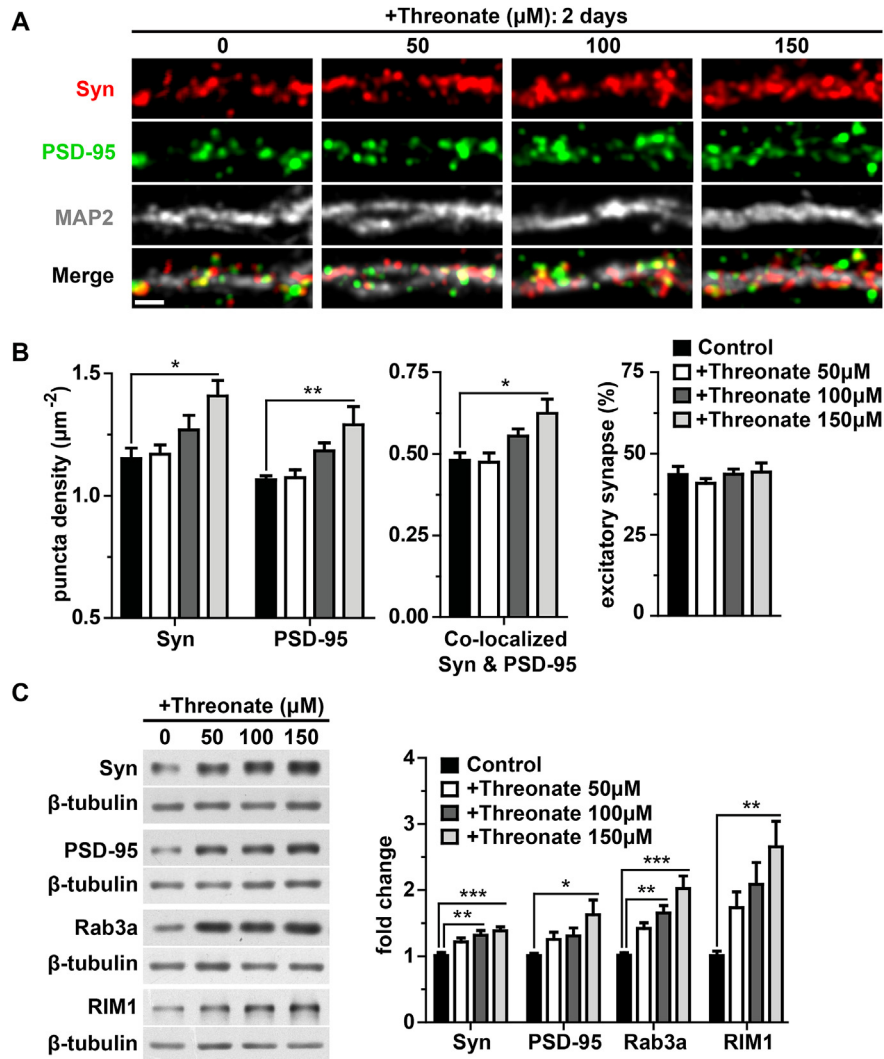


Fig. 3. Enhancement of synaptic density by threonate. Hippocampal neuronal cultures were treated with threonate for 2 days. (A) Representative fluorescent images of synaptic terminal marker synaptophysin (Syn) and spine marker PSD-95 of controls ($n = 5$) and threonate-treated hippocampal neurons ($n = 4-6$) at varying threonate concentrations (0–150 μM); n means number of coverslips, 5–7 images for one coverslip, and 50–60 branches for one image. Scale bar represents 2 μm . (B) Quantification of Syn and PSD-95-immunostained puncta. Left panel) the absolute number of Syn and PSD-95; Middle panel) amount of Syn & PSD-95 co-localized; Right panel) the percentage (%) of excitatory synapses (% of excitatory synapses was calculated as the density of co-localized Syn and PSD-95 puncta divided by the density of total Syn puncta). One-way ANOVA compared number of puncta in threonate-treated neurons to controls; * $p < 0.05$; ** $p < 0.01$. (C) Western blot and quantitative analysis of synaptic proteins Syn, PSD-95, Rab3a and RIM1 expression in hippocampal neuronal cultures treated with threonate (0–150 μM). β -tubulin was used as a loading control. Data is represented as fold change relative to control (0 μM threonate). One-way ANOVA and Bonferroni's post hoc test; * $p < 0.05$, ** $p < 0.01$, *** $p < 0.001$; n means number of separate cultures.

threonate was the only one able to increase intracellular $[\text{Mg}^{2+}]$ ($F_{5,19} = 3.455$, $p = 0.0218$; Fig. 6A, B).

Next, we compared these molecules in their ability to increase functional synapse density in hippocampal neurons. After 2 days of treatment, only threonate was able to significantly increase functional terminal density ($F_{5,25} = 10.99$, $p < 0.0001$; Fig. 6C, D). Citrate, gluconate, malate, and glycinate treatments had no significant effects. The fact that only threonate resulted in a change in intracellular $[\text{Mg}^{2+}]$ and functional terminal density gave insight into the underlying mechanistic pathway by which threonate enhances synaptic changes.

3.6. GLUTs necessary for threonate-induced synaptic changes and increase of functional synapse density

Since only threonate was effective at increasing intracellular

$[\text{Mg}^{2+}]$ and functional synaptic density, we focused on its transport mechanisms. Elevated intracellular $[\text{Mg}^{2+}]$ might be due to increased Mg^{2+} influx, reduced Mg^{2+} efflux, and/or release of Mg^{2+} from organelles (Shindo et al., 2010). We tested whether the elevation of intracellular Mg^{2+} by threonate depends on Mg^{2+} influx. Since Mg^{2+} influx is driven by a concentration gradient between extracellular and intracellular Mg^{2+} , a significant reduction of extracellular Mg^{2+} will diminish the gradient, preventing Mg^{2+} influx. If the threonate effects disappear under low extracellular $[\text{Mg}^{2+}]$ conditions (0.1 mM), then the effects of threonate are likely mediated through Mg^{2+} influx.

In line with previous experiments, threonate treatment for 4 h, at 0.6 mM extracellular $[\text{Mg}^{2+}]$, induced a significant ~27% increase of intracellular $[\text{Mg}^{2+}]$ ($p < 0.001$). When extracellular $[\text{Mg}^{2+}]$ was reduced to 0.1 mM for 4 h, intracellular $[\text{Mg}^{2+}]$ did not decline (Fig. 7A, B), but, addition of threonate no longer induced elevation

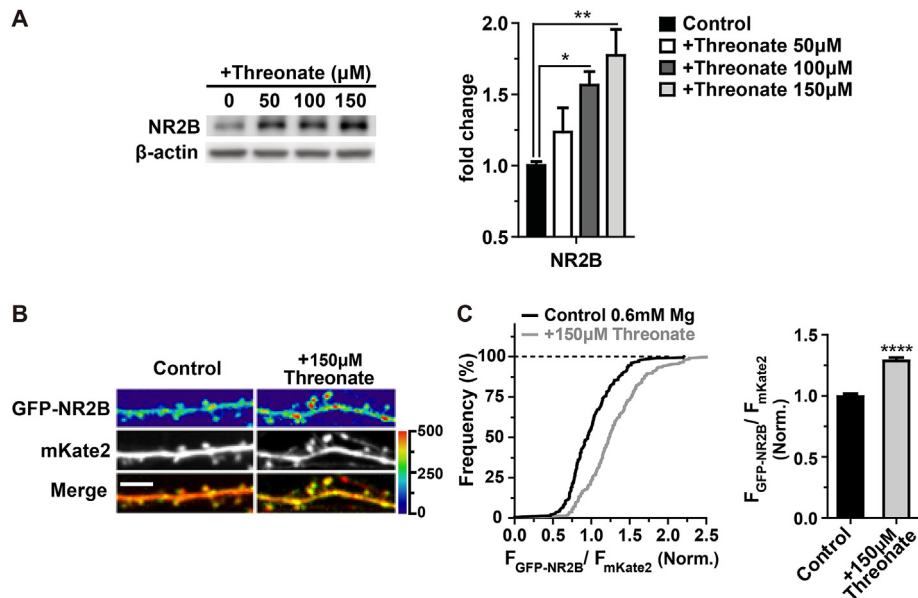


Fig. 4. Upregulation of NR2B-containing NMDAR by threonate. (A) Western blot and quantitative analysis for NR2B-containing NMDAR protein in hippocampal neurons. β -actin was used as a loading control. One-way ANOVA and Bonferroni's post hoc test; * $p < 0.05$; ** $p < 0.01$. (B) Representative images with GFP-NR2B (pseudo-color) and mKate2 (gray) of hippocampal neurons following treatment with threonate (150 μ M) for 2 days. Scale bar represents 5 μ m. (C) Expression of NR2B in each dendritic spine was calculated from images represented in B (197 spines for control, and 206 spines for threonate-treated neurons on 3 coverslips for each condition). The ratio of $F_{\text{GFP-NR2B}}/F_{\text{mKate2}}$ in each individual spine represents the quantify of NR2B expression; F means fluorescence intensity. The distribution of expression of NR2B in spines is shown in the left panel, and mean expression of NR2B is shown in the histogram in the right panel. $F_{\text{GFP-NR2B}}/F_{\text{mKate2}}$ values were normalized to control group. Kolmogorov-Smirnov test, $p < 0.0001$.

of intracellular $[\text{Mg}^{2+}]$ (Fig. 7A, B). Similarly, reducing extracellular $[\text{Mg}^{2+}]$ to 0.1 mM for 4 h did not reduce functional terminal density (Fig. 7C, D) relative to control extracellular $[\text{Mg}^{2+}]$ (Fig. 7Ca, D). However, this condition prevented threonate from increasing functional terminal density (Fig. 7Cd, D).

These results indicate that threonate elevated intracellular $[\text{Mg}^{2+}]$ of hippocampal neurons most likely by increasing net flux of Mg^{2+} into the neuron, resulting in the increase of functional terminal density; although, the possibility that threonate promotes functional synapse density independently of Mg^{2+} cannot be ruled out.

Our focus was to identify the transporter that underlies threonate-mediated Mg^{2+} influx. There are no known transporters for threonate, but because threonate is a derivative of ascorbic acid/DHA, we investigated if threonate acted through ascorbic acid and/or DHA transporters. Ascorbic acid is transported by glucose transporters (GLUTs) (Rumsey et al., 1997) and sodium-dependent vitamin C transporter 2 (SVCT2) (Harrison and May 2009; Savini et al., 2008), which are highly expressed in the CNS (McEwen and Reagan, 2004; Tsukaguchi et al., 1999).

To specifically target GLUTs and SVCT2, we utilized cytochalasin B (CB) and Phloretin, because of their ability to inhibit GLUTs (Yu et al., 1993) and SVCT2 (Gess et al., 2010), respectively. While short-term incubation (4 h) of hippocampal neuronal cultures with threonate increased intracellular $[\text{Mg}^{2+}]$ (29.6%, $p < 0.001$), this threonate-mediated increase was prevented by the addition of CB. CB alone did not alter intracellular $[\text{Mg}^{2+}]$ relative to control (Fig. 7E, F). In contrast, treatment with Phloretin did not affect the ability of threonate to significantly increase intracellular $[\text{Mg}^{2+}]$ (23.5%, $p < 0.001$) (Fig. 7E, F). These results suggest an involvement of GLUTs, but not SVCT2, in the modulation of intracellular $[\text{Mg}^{2+}]$ by threonate which can lead to augmentation of functional terminal density.

We then checked whether blocking GLUTs or SVCT2 by CB or Phloretin would affect the ability of threonate to elevate functional

terminal density of hippocampal neurons. CB treatment alone did not affect the density of functional terminals relative to control; however, in the presence of CB, threonate treatment was unable to elevate functional terminal density (Fig. 7Gd, H), similar to the effects of CB on threonate-mediated increase of intracellular $[\text{Mg}^{2+}]$. Addition of Phloretin significantly decreased functional terminal density (10.5%, $p < 0.01$) in hippocampal cultures, and was unable to block threonate-mediated increase of functional terminal density relative to control (20.4%) (Fig. 7Gf, H). Altogether, we conclude that GLUTs mediate threonate-induced increases in neuronal intracellular $[\text{Mg}^{2+}]$ and functional synapse density.

3.7. Threonate upregulated expression level of Syn and PSD-95 in human neural stem cell-derived neurons

To help understand the potential ramifications of the present study in human, we examined the effects of threonate on synaptic changes in human stem cell-derived neurons. In a separate study, we found plasma threonate concentrations were similar between human and rat; but human CSF threonate concentrations (100–300 μ M), were much higher than those in rat (internal observation). Threonate function may vary between rodent and human due to species differences in ascorbate synthesis and plasma and CSF concentrations (Burns, 1957; Harrison and May 2009; Horowitz et al., 1952; Jackel et al., 1950; Miele and Fillenz, 1996; Pauling, 1970; Reiber et al., 1993; Schenk et al., 1982). To test this, human neuronal cultures were derived from human neural stem cells (hNSC) (Shi and Jiao, 2012). We evaluated the effects of threonate on human neurons using Western blot to check the expression of pre- and postsynaptic proteins, which is supposed to be proportional to the number of synapses (Glantz et al., 2007).

Fig. 8A shows the experimental protocol used for deriving neurons from hNSC. In this cell line, structural and functional synapses are present at day 45 following induction of differentiation (Shi and Jiao, 2012). We observed glutamatergic synapses

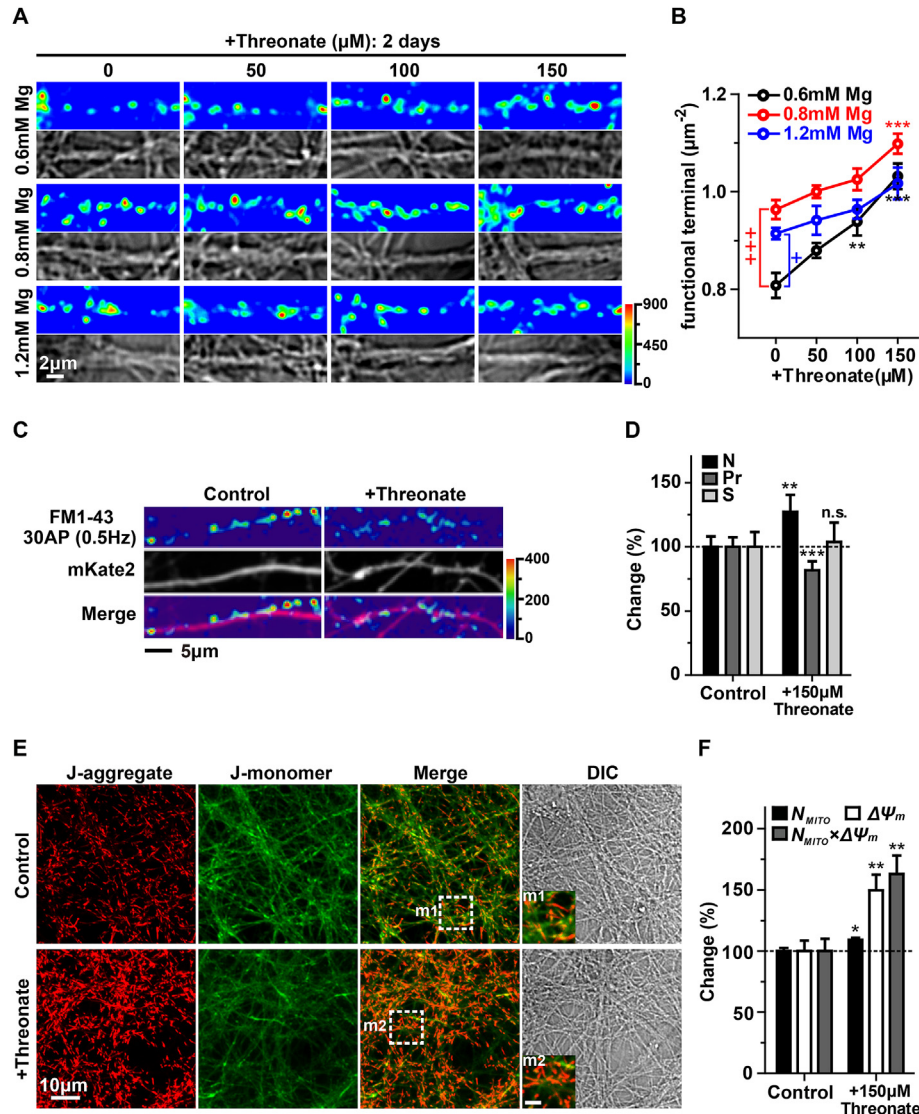


Fig. 5. Threonate increases functional presynaptic terminal density and enhances mitochondrial function. (A) Representative fluorescent FM1-43 (pseudo-colored) and DIC (gray) images of control (0 μM threonate) and threonate-treated (50–150 μM) neurons. Each FM+ puncta is a functional synaptic terminal. (B) Functional terminal density was calculated from images represented in A (see methods, $n = 5-7$ coverslips). One-way ANOVA compared functional terminal density in 0.6 mM Mg ($n = 7$), 0.8 mM Mg ($n = 5$), and 1.2 mM Mg ($n = 5$) to 0 μM threonate. For each $[\text{Mg}^{2+}]_o$ (0.6, 0.8 or 1.2 mM), threonate-treated neurons (50–150 μM ; $n = 5-7$) were compared to controls (0 μM), separately, using one-way ANOVA and Bonferroni's post hoc test. $+p < 0.05$, $+++p < 0.001$; $**p < 0.01$, $***p < 0.001$. (C) Representative fluorescent FM1-43 (pseudo-color) and mKate2 (gray) images of hippocampal neurons following treatment with threonate (150 μM) for 2 days (mKate2 was used to calculate the total area of dendrites). Puncta number per μm^2 of dendrite was calculated to determine the density of terminals (N). The intensity of FM+ puncta is proportional to the probability of transmitter release (Pr). Synaptic strength (S) to a unit area of dendrite is calculated as $N \times Pr$. (D) N , Pr , and S of terminals were calculated from images represented in A ($n = 3$ coverslips, each coverslip contained 9 areas of interest). Student t tests for N , Pr , and S compared threonate-treated versus control conditions, $**p < 0.01$, $***p < 0.001$. (E) Representative fluorescent images of hippocampal neuronal cultures dyed with JC-1 to determine mitochondrial function following treatment with threonate (150 μM) for 2 days. Mitochondrial transmembrane potential ($\Delta\Psi_m$) was measured by ratio of JC-1 aggregate (red) and monomer (green). Dashed boxes ($m1$ and $m2$) are high magnifications of regions marked in the low magnification images. Scale bar represents 2 μm . (F) Histogram of average mitochondrial density (N_{MITO}), $\Delta\Psi_m$, and functional status ($N_{\text{MITO}} \times \Delta\Psi_m$) (Control, 0.6 mM Mg, $n = 8$ coverslips; threonate, $n = 5$ coverslips). Unpaired t test compared parameters in threonate-treated neurons to controls; $**p < 0.01$.

(yellow puncta) located surrounding dendritic branches (MAP2, gray) at day 80, via fluorescent co-localization of presynaptic protein Syn (red puncta) and postsynaptic protein PSD-95 (green puncta) (Fig. 8Ac-g), and treated the human neurons with threonate at day 90. Similar to our findings in cultured rat hippocampal neurons, threonate treatment significantly increased Syn and PSD-95 expression in a dose-dependent manner (Syn, $F_{4,67} = 4.499$, $p = 0.0028$; PSD-95, $F_{4,44} = 4.221$, $p = 0.0056$; Fig. 8B, C). Interestingly, compared to the rat dose response curve, in human neurons, the threonate dose response curve was shifted toward a higher concentration, such that even at 400 μM , a concentration

higher than human physiological concentration, the effects of threonate continued to increase. This shift seems to be matched with the higher concentration of threonate in human CSF.

4. Discussion

Threonate is an endogenous small molecule shown to have a possible physiological function in the periphery - supporting bone health. However, until now, there have been no reports of the presence of or a physiological role for threonate in the CNS. In the current study, we showed for first time that threonate is present in

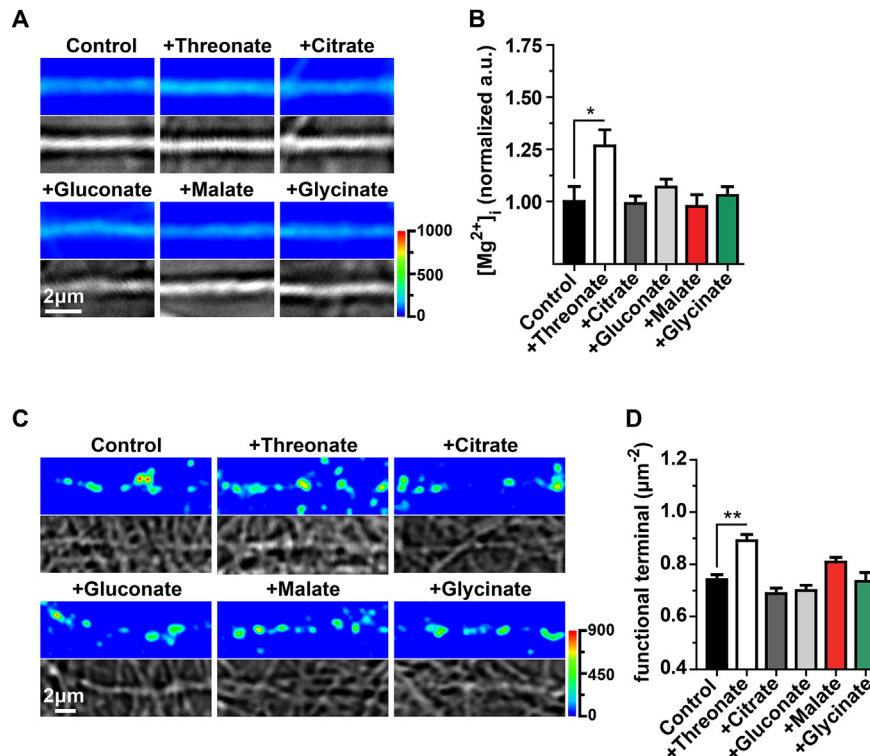


Fig. 6. Comparison of effects of various anions on $[Mg^{2+}]_i$ and functional synaptic density. (A) Representative MgGreen (pseudo-colored) and DIC (gray) fluorescent images of individual branches after 2 day treatment with threonate or threonate analogs at 0.6 mM $[Mg^{2+}]_o$ (control). (B) Histogram of average $[Mg^{2+}]_i$, calculated from the MgGreen and DIC images represented in A. All compound-treated neurons ($n = 4$ coverslips) were compared to controls ($n = 5$ coverslips). One-way ANOVA and Bonferroni's post hoc test; * $p < 0.05$. (C) Representative fluorescent FM1-43 (pseudo-colored) and DIC (gray) images of hippocampal neuronal cultures following treatment with threonate or threonate analogs for 2 days at 0.6 mM $[Mg^{2+}]_o$ (control). (D) Histogram of functional terminal density calculated from images represented in C ($n = 5$ –6 coverslips). All compound-treated neurons were compared to controls. One-way ANOVA and Bonferroni's post hoc test; ** $p < 0.01$.

the rat CSF and human CSF (data not shown), surprisingly at an approximate 5-fold higher concentration than in the periphery. We identified threonate as a unique molecule that can efficiently regulate structural and functional synaptic density in the CNS. Here we show that threonate treatment of hippocampal neuronal cultures increased mitochondrial function, proteins critical for synaptic plasticity, and structural and functional synapse density, in a dose-dependent manner. Importantly, we also identified the likely signaling mechanism by which threonate affects functional synapse density. We show that threonate elevates neuronal intracellular $[Mg^{2+}]_i$, which acts as a “second messenger” for threonate in regulating synapse density (Zhou and Liu, 2015).

We have carried out experiments to decipher the possible mechanism underlying the elevation of neuronal intracellular $[Mg^{2+}]_i$ by threonate, which could be due to increased Mg^{2+} influx or decreased Mg^{2+} efflux. We observed that when we dropped extracellular $[Mg^{2+}]_o$ to 0.1 mM in an attempt to reduce the driving force for Mg^{2+} influx, threonate treatment no longer elevated intracellular $[Mg^{2+}]_i$. These results are most compatible with the interpretation that threonate promotes Mg^{2+} influx.

We conducted several experiments to identify the possible channel responsible for threonate-mediated Mg^{2+} influx into neurons. The candidates we considered were channels that have high potential to transport threonate, including GLUTs and SVCT2, based on threonate's structure and related chemical precursors. Threonate is formed by the spontaneous conversion of the ascorbic acid oxidation product dehydroascorbic acid (DHA) into oxalic acid and threonic acid (Kallner et al., 1985; Thornalley, 1998). GLUTs have specificity for the threonate precursor DHA and is also known to transport monosaccharides and other small carbon compounds

via passive facilitated transport, whereas SVCT2 has specificity for ascorbic acid (Augustin, 2010; Rumsey et al., 1999). Blocking GLUTs, but not SVCT2, suppressed both threonate-mediated Mg^{2+} influx and increase of functional synaptic density. Although the CB experiments suggest that GLUTs are responsible for threonate-mediated influx of Mg^{2+} into neurons, since the specificity of CB to GLUTs cannot be completely confirmed, additional experiments, such as siRNA knock-down, are required before we can conclusively conclude that it is GLUTs that mediate the action of threonate on intracellular Mg^{2+} concentration. Nevertheless, given the chemical structure similarity between DHA and threonate, we speculate that GLUTs facilitate threonate transport into the cell while co-transporting Mg^{2+} .

Because the drug we used to block GLUTs is not specific for a particular GLUT, we do not know which of the GLUTs expressed in the brain (GLUTs 1–4, 6, 8, 10, 13) are capable of threonate-mediated transport of Mg^{2+} into neurons. Although, among the brain expressed GLUTs, GluTs 1 and 3 are known to transport DHA, suggesting that they might also be responsible for threonate transport (Rumsey et al., 1997). GluT3, but not GluT1, is highly constitutively expressed on hippocampal neurons as the primary mediator of neuronal glucose uptake (Leino et al., 1997; Maher et al., 1991; Nagamatsu et al., 1992; Vannucci et al., 1997). Therefore, threonate-induced transport of Mg^{2+} into hippocampal neurons likely occurred primarily through GluT3 in our experiments. Interestingly, GluT1 is highly expressed on endothelial cells of the blood brain barrier, important for glucose uptake into the brain (Koranyi et al., 1991; Simpson et al., 2001; Yeh et al., 2008). Therefore, GluT1 may be responsible for the observed threonate-mediated transport of Mg^{2+} into the brain (Slutsky et al., 2010).

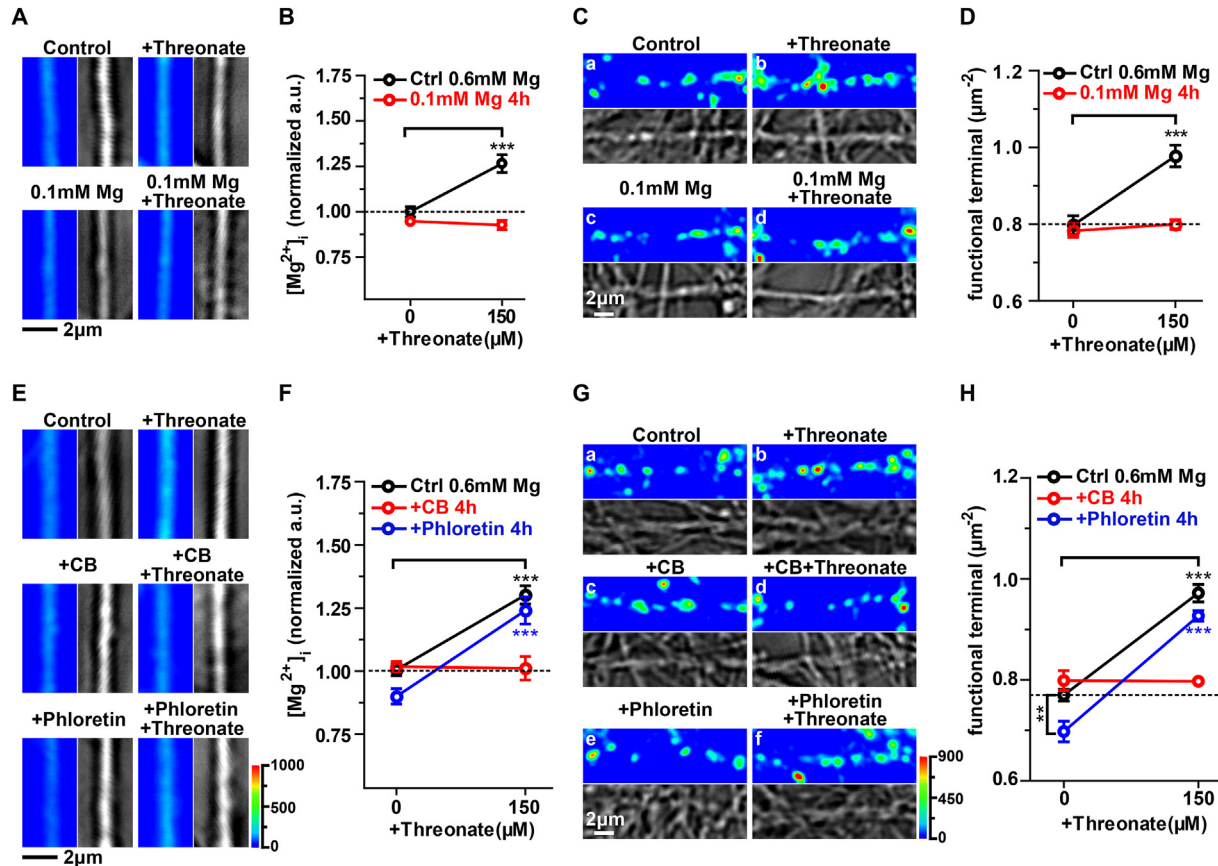


Fig. 7. Glucose transporters (GLUTs) are essential for threonate-induced synaptic changes and increase of functional synapse density. (A) Representative MgGreen (pseudo-colored) and DIC (gray) fluorescent images of individual branches after 4 h treatment with or without threonate (150 μM) in neuronal cultures at 0.6 mM or 0.1 mM $[Mg^{2+}]_o$. (B) Histogram of average $[Mg^{2+}]_i$ calculated from the MgGreen and DIC images represented in A. Two-way ANOVA compared $[Mg^{2+}]_i$ at 0.6 and 0.1 mM $[Mg^{2+}]_o$ with threonate to without threonate, with Bonferroni's post hoc test ($n = 4-10$ coverslips). (C) Representative fluorescent FM1-43 (pseudo-colored) and DIC (gray) images of hippocampal neuronal cultures following treatment with threonate (150 μM, 4 h) or control (0 μM threonate) in 0.6 mM $[Mg^{2+}]_o$ (control) or in 0.1 mM $[Mg^{2+}]_o$. (D) Histogram of functional terminal density calculated from images represented in C ($n = 6$ coverslips). Two-way ANOVA compared functional terminal density at 0.6 and 0.1 mM $[Mg^{2+}]_o$ with threonate to without threonate, with Bonferroni's post hoc test. (E–H) Hippocampal cultures were incubated with threonate, cytochalasin B (CB; GLUTs inhibitor, 10 μM), and/or Phloretin (SVCT2 inhibitor, 150 μM) for 4 h. (E) Representative MgGreen (pseudo-colored) and DIC (gray) fluorescent images of individual branches following 4 h treatment with threonate (150 μM) or control (0 μM threonate) with or without CB or Phloretin. (F) $[Mg^{2+}]_i$ was calculated as normalized $F_{(a.u.)}$ by dividing each branch's MgGreen $F_{(a.u.)}$ by its mean diameter (measured from DIC images), from images represented in E. Two-way ANOVA was used to compare $[Mg^{2+}]_i$ in different conditions, Bonferroni's post-hoc test ($n = 4-17$ coverslips). (G) Representative fluorescent FM1-43 (pseudo-colored) and DIC (gray) images of hippocampal neuronal cultures after threonate (150 μM) or control (0 μM threonate) treatment with CB or Phloretin. (H) Histogram of functional terminal density calculated from images represented in G. Two-way ANOVA compared effect of threonate, CB or Phloretin on functional terminal density to controls, and effect of threonate on functional terminal density in the presence of CB or Phloretin, respectively, with Bonferroni's post-hoc test ($n = 6-15$ coverslips), ** $p < 0.01$, *** $p < 0.001$.

Maintaining a sufficient amount of synapses is essential for brain function. Indeed, the decline of cognitive function during aging is strongly correlated with the degree of synapse loss (Morrison and Baxter, 2012). Identifying the endogenous molecule that regulates synapse density will likely be of broad significance. So far, only a handful of endogenous molecules have been shown to have a role in upregulating synapse density. For example, estrogen can efficiently increase synapse density in hippocampal neurons (Mukai et al., 2010). Acetyl-L-carnitine (ACL), a derivative of the constitutively expressed fatty acid transporter L-carnitine, can potentially promote hippocampal dendritic spine density (Kocsis et al., 2014). The current study shows that threonate might be an important constitutively present molecule in the CSF required for maintaining high synapse density.

Translationally, a threonate or Mg^{2+} compound might be useful to increase synapse density and promote learning and memory. Surprisingly, in our previous animal experiments, we found that treatment with either threonate or Mg^{2+} but without the other was ineffective (Slutsky et al., 2010). Only treatment with the

combination of threonate and Mg^{2+} as a single compound can elevate memory ability. While oral treatment with threonate and Mg^{2+} (in the form of L-TAMS) can efficiently increase synapse density and memory ability in both aged rats and late stage AD model mice (Li et al., 2014; Slutsky et al., 2010), threonate treatment without Mg^{2+} (in the form of NaT) and Mg^{2+} treatment without threonate (in the form of Mg^{2+} -chloride, -citrate, -glycinate, and -gluconate) fails to increase short- or long-term memory ability (Slutsky et al., 2010).

If threonate is effective in increasing intraneuronal Mg^{2+} and synapse density in cultured hippocampal neurons, it is curious why it does not have an effect in the intact animal. One possible explanation is that threonate might not be able to promote Mg^{2+} influx into neurons without a simultaneous increase of extracellular brain Mg^{2+} supply. This is because Mg^{2+} as a signaling molecule is unique in that the majority of Mg^{2+} is stored inside the cell and there is a relatively very small amount of Mg^{2+} in the extracellular space. Therefore, a large influx of Mg^{2+} can lead to a significant reduction of extracellular Mg^{2+} , thereby reducing the

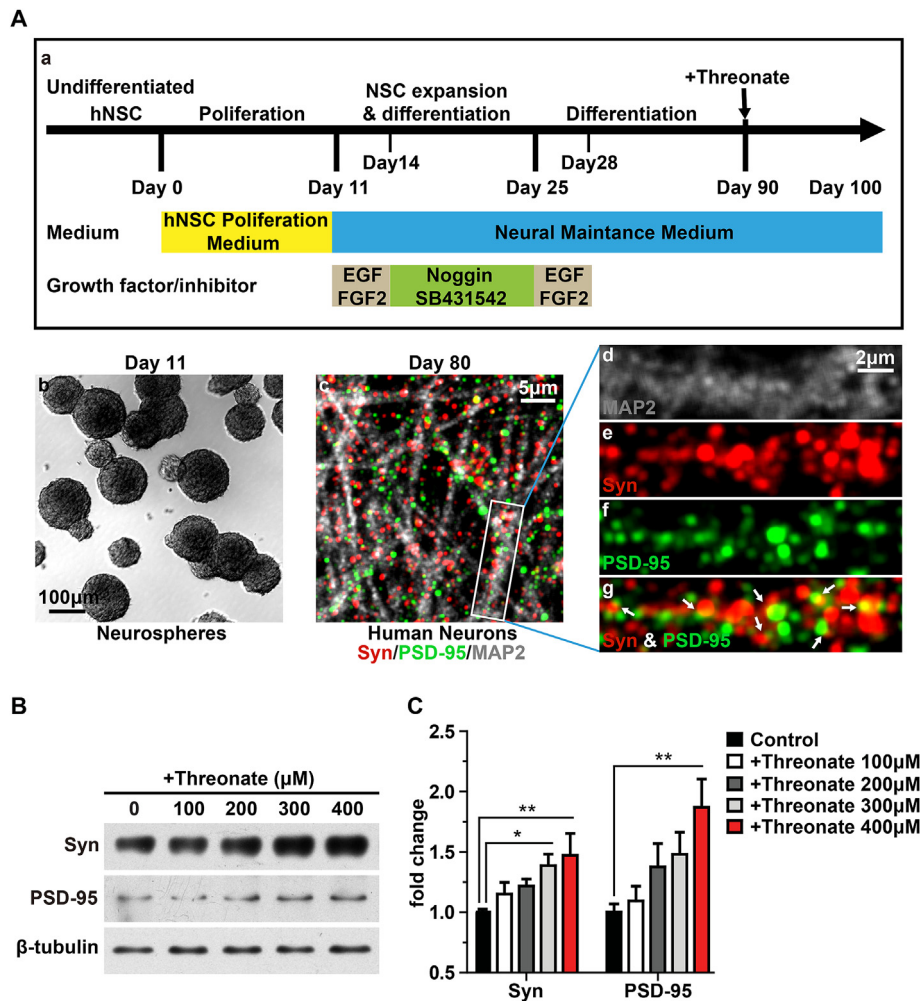


Fig. 8. Elevating threonate increased expression of Syn and PSD-95 in human neurons. (A) (a) Schematic of protocol for differentiation of human neural stem cells (hNSC) into neurons and subsequent threonate treatment. (b) Neurospheres at optimal size for passaging after proliferation. (c–g) Confocal microscopy images of immunofluorescent staining for hNSC-derived neurons. (c) Images of dendrites (MAP2, gray) showing localization of foci of the excitatory synapse. Physical synapses (arrows in g) were identified by juxtaposition of pre- (Syn; e, red) and postsynaptic (PSD-95; f, green) proteins on dendritic branches (d, gray). (B–C) Representative Western blot (B) and quantified histogram (C) of Syn ($n = 9–18$) and PSD-95 ($n = 6–13$) in control and threonate-treated hNSC-derived neurons. β -tubulin was used as a loading control. Data are presented as fold change relative to control. One-way ANOVA and Bonferroni's post hoc test; * $p < 0.05$; ** $p < 0.01$.

driving force of Mg^{2+} , preventing further influx. This phenomenon can be observed with insulin treatment. Insulin promotes Mg^{2+} influx into the cell, significantly reducing extracellular Mg^{2+} . For example, plasma Mg^{2+} levels initially decrease significantly following an insulin injection, but can be prevented when insulin is injected with Mg^{2+} supplementation, such as from a meal (Paolisso et al., 1986). Since the amount of total extracellular brain Mg^{2+} is low (Ramadan et al., 1989), threonate treatment without concurrent Mg^{2+} treatment, like with insulin treatment, could quickly reduce CSF Mg^{2+} , resulting in a reduction of the driving force for all Mg^{2+} channels, limiting the amount of Mg^{2+} influx that threonate can promote. This might explain why threonate treatment alone does not work *in vivo*, whereas in culture, where the extracellular $[Mg^{2+}]$ is essentially clamped, threonate treatment effectively increases intracellular $[Mg^{2+}]$.

Similar to the effects of increasing CSF threonate without increasing Mg^{2+} , increasing CSF Mg^{2+} without increasing CSF threonate will also not be effective. One cannot limitlessly elevate extracellular brain Mg^{2+} in order to elevate intracellular $[Mg^{2+}]$, as the relationship between extracellular and intracellular $[Mg^{2+}]$,

and the relationship of extracellular $[Mg^{2+}]$ and synapse density are bell-shaped. As shown in Fig. 2 and Fig. 5, when the extracellular $[Mg^{2+}]$ is increased beyond 0.8 mM, intracellular $[Mg^{2+}]$ and synapse density decreased.

The greatest increase *in vitro* of intracellular $[Mg^{2+}]$ and functional synapse density occurred with the concurrent increase of threonate and extracellular $[Mg^{2+}]$ (Figs. 2B and 5A, B). *In vivo*, threonate and Mg^{2+} oral treatment (L-TAMS) increased brain threonate by approximately 50% (Fig. 1C) and CSF Mg^{2+} by approximately 15%, leading to an increase of synapse density by as much as 67% (Slutsky et al., 2010). The current study provides more mechanistic insight into the therapeutic potential of L-TAMS for cognitive impairment. A recent double-blinded placebo-controlled clinical study showed promise for L-TAMS in treating cognitive impairment in humans (Liu et al., 2015).

Acknowledgments

This study was supported by the Tsinghua University Initiative Scientific Research Program 20131080156 (G.L.). We thank

Fangzhou Liao for assistance in threonate concentration testing, and Zhou Hang for carrying out experiments and analyzing data in Fig. 4B, C and Fig. 5C, D.

Appendix A. Supplementary data

Supplementary data related to this article can be found at <http://dx.doi.org/10.1016/j.neuropharm.2016.05.006>.

References

- Andrasi, E., Pali, N., Molnar, Z., Kosel, S., 2005. Brain aluminum, magnesium and phosphorus contents of control and Alzheimer-diseased patients. *J. Alzheimers Dis.* 7, 273–284.
- Augustin, R., 2010. The protein family of glucose transport facilitators: it's not only about glucose after all. *IUBMB Life* 62, 315–333.
- Buckman, J.F., Reynolds, I.J., 2001. Spontaneous changes in mitochondrial membrane potential in cultured neurons. *J. Neurosci.* 21, 5054–5065.
- Burns, J.J., 1957. Missing step in man, monkey and guinea pig required for the biosynthesis of L-ascorbic acid. *Nature* 180, 553.
- Cilliler, A.E., Ozturk, S., Ozbakir, S., 2007. Serum magnesium level and clinical deterioration in Alzheimer's disease. *Gerontology* 53, 419–422.
- Deutsch, J.C., Butler, J.A., Marsh, A.M., Ross, C.A., Norris, J.M., 1999. Rapid mass spectrometric analysis for ascorbate and related organic acids in small volumes of plasma for use in pediatric subjects. *J. Chromatogr. B Biomed. Sci. Appl.* 726, 79–84.
- Fox, C.H., Timm Jr., E.A., Smith, S.J., Touyz, R.M., Bush, E.G., Wallace, P.K., 2007. A method for measuring intracellular free magnesium concentration in platelets using flow cytometry. *Magnes. Res.* 20, 200–207.
- Gess, B., Lohmann, C., Halfter, H., Young, P., 2010. Sodium-dependent vitamin C transporter 2 (SVCT2) is necessary for the uptake of L-ascorbic acid into Schwann cells. *Glia* 58, 287–299.
- Glantz, L.A., Gilmore, J.H., Hamer, R.M., Lieberman, J.A., Jarskog, L.F., 2007. Synaptophysin and postsynaptic density protein 95 in the human prefrontal cortex from mid-gestation into early adulthood. *Neuroscience* 149, 582–591.
- Harding, J.J., Hassett, P.C., Rixon, K.C., Bron, A.J., Harvey, D.J., 1999. Sugars including erythronic and threonic acids in human aqueous humour. *Curr. Eye Res.* 19, 131–136.
- Harrison, F.E., May, J.M., 2009. Vitamin C function in the brain: vital role of the ascorbate transporter SVCT2. *Free Radic. Biol. Med.* 46, 719–730.
- He, J.H., Tong, N.W., Li, H.Q., Wu, J., 2005. Effects of L-threonate on bone resorption by osteoclasts in vitro. *Sichuan Da Xue Xue Bao Yi Xue Ban* 36, 225–228.
- Hertrampf, E., Olivares, M., 2004. Iron amino acid chelates. *Int. J. Vitam. Nutr. Res.* 74, 435–443.
- Hoffmann, G.F., Meier-Augenstein, W., Stockler, S., Surtees, R., Rating, D., Nyhan, W.L., 1993. Physiology and pathophysiology of organic acids in cerebrospinal fluid. *J. Inher. Metab. Dis.* 16, 648–669.
- Horowitz, H.H., Doerschuk, A.P., King, C.G., 1952. The origin of L-ascorbic acid in the albino rat. *J. Biol. Chem.* 199, 193–198.
- Hunt, C.A., Schenker, L.J., Kennedy, M.B., 1996. PSD-95 is associated with the postsynaptic density and not with the presynaptic membrane at forebrain synapses. *J. Neurosci.* 16, 1380–1388.
- Jack Jr., C.R., Wiste, H.J., Weigand, S.D., Knopman, D.S., Vemuri, P., Mielke, M.M., Lowe, V., Senjem, M.L., Gunter, J.L., Machulda, M.M., Gregg, B.E., Pankratz, V.S., Rocca, W.A., Petersen, R.C., 2015. Age, sex, and APOE epsilon4 effects on memory, brain structure, and beta-amyloid across the adult life span. *JAMA Neurol.* 72, 511–519.
- Jackel, S.S., Mosbach, E.H., Burns, J.J., King, C.G., 1950. The synthesis of l-ascorbic acid by the albino rat. *J. Biol. Chem.* 186, 569–579.
- Kaech, S., Banker, G., 2006. Culturing hippocampal neurons. *Nat. Protoc.* 1, 2406–2415.
- Kallner, A., Hornig, D., Pellikar, R., 1985. Formation of carbon dioxide from ascorbate in man. *Am. J. Clin. Nutr.* 41, 609–613.
- Kocsis, K., Knapp, L., Gellert, L., Olah, G., Kis, Z., Takakuwa, H., Iwamori, N., Ono, E., Toldi, J., Farkas, T., 2014. Acetyl-L-carnitine normalizes the impaired long-term potentiation and spine density in a rat model of global ischemia. *Neuroscience* 269, 265–272.
- Koranyi, L., Bourey, R.E., James, D., Mueckler, M., Fiedorek Jr., F.T., Permutt, M.A., 1991. Glucose transporter gene expression in rat brain: pretranslational changes associated with chronic insulin-induced hypoglycemia, fasting, and diabetes. *Mol. Cell Neurosci.* 2, 244–252.
- Kwack, M.H., Ahn, J.S., Kim, M.K., Kim, J.C., Sung, Y.K., 2010. Preventable effect of L-threonate, an ascorbate metabolite, on androgen-driven balding via repression of dihydrotestosterone-induced dickkopf-1 expression in human hair dermal papilla cells. *BMB Rep.* 43, 688–692.
- Kwack, M.H., Sung, Y.K., Chung, E.J., Im, S.U., Ahn, J.S., Kim, M.K., Kim, J.C., 2008. Dihydrotestosterone-inducible dickkopf 1 from balding dermal papilla cells causes apoptosis in follicular keratinocytes. *J. Invest. Dermatol.* 128, 262–269.
- Lawson, A.M., Chalmers, R.A., Watts, R.W., 1976. Urinary organic acids in man. I. Normal patterns. *Clin. Chem.* 22, 1283–1287.
- Le Roux, N., Amar, M., Moreau, A., Fossier, P., 2007. Involvement of NR2A- or NR2B-containing N-methyl-D-aspartate receptors in the potentiation of cortical layer 5 pyramidal neurone inputs depends on the developmental stage. *Eur. J. Neurosci.* 26, 289–301.
- Leino, R.L., Gerhart, D.Z., van Bueren, A.M., McCall, A.L., Drewes, L.R., 1997. Ultrastructural localization of GLUT 1 and GLUT 3 glucose transporters in rat brain. *J. Neurosci. Res.* 49, 617–626.
- Li, W., Yu, J., Liu, Y., Huang, X., Abumaria, N., Zhu, Y., Huang, X., Xiong, W., Ren, C., Liu, X.G., Chui, D., Liu, G., 2014. Elevation of brain magnesium prevents synaptic loss and reverses cognitive deficits in Alzheimer's disease mouse model. *Mol. Brain* 7, 65.
- Liu, G., Choi, S., Tsien, R.W., 1999. Variability of neurotransmitter concentration and nonsaturation of postsynaptic AMPA receptors at synapses in hippocampal cultures and slices. *Neuron* 22, 395–409.
- Liu, G., Tsien, R.W., 1995. Properties of synaptic transmission at single hippocampal synaptic boutons. *Nature* 375, 404–408.
- Liu, G., Weinger, J.G., Lu, Z.L., Xue, F., Sadeghpour, S., 2015. Efficacy and safety of MMFS-01, a synapse density enhancer, for treating cognitive impairment in older adults: a randomized, double-blind, placebo-controlled trial. *J. Alzheimers Dis.* 49, 971–990.
- Lowenstein, P.R., Shering, A.F., Morrison, E., Tomasec, P., Bain, D., Jacob, T.J., Wu, J., Prescott, A., Castro, M.G., 1995. Synaptogenesis and distribution of presynaptic axonal varicosities in low density primary cultures of neocortex: an immunocytochemical study utilizing synaptic vesicle-specific antibodies, and an electrophysiological examination utilizing whole cell recording. *J. Neurocytol.* 24, 301–317.
- Luo, J.H., Fu, Z.Y., Losi, G., Kim, B.G., Prybylowski, K., Vissel, B., Vicini, S., 2002. Functional expression of distinct NMDA channel subunits tagged with green fluorescent protein in hippocampal neurons in culture. *Neuropharmacology* 42, 306–318.
- Maher, F., Davies-Hill, T.M., Lysko, P.G., Henneberry, R.C., Simpson, I.A., 1991. Expression of two glucose transporters, GLUT1 and GLUT3, in cultured cerebellar neurons: evidence for neuron-specific expression of GLUT3. *Mol. Cell Neurosci.* 2, 351–360.
- McEwen, B.S., Reagan, L.P., 2004. Glucose transporter expression in the central nervous system: relationship to synaptic function. *Eur. J. Pharmacol.* 490, 13–24.
- Miele, M., Fillenz, M., 1996. In vivo determination of extracellular brain ascorbate. *J. Neurosci. Methods* 70, 15–19.
- Monroe, D.G., McGee-Lawrence, M.E., Oursler, M.J., Westendorf, J.J., 2012. Update on Wnt signaling in bone cell biology and bone disease. *Gene* 492, 1–18.
- Morrison, J.H., Baxter, M.G., 2012. The ageing cortical synapse: hallmarks and implications for cognitive decline. *Nat. Rev. Neurosci.* 13, 240–250.
- Mukai, H., Kimoto, T., Hojo, Y., Kawato, S., Murakami, G., Higo, S., Hatanaka, Y., Ogiue-Ikeda, M., 2010. Modulation of synaptic plasticity by brain estrogen in the hippocampus. *Biochim. Biophys. Acta* 1800, 1030–1044.
- Nagamatsu, S., Kornhauser, J.M., Burant, C.F., Seino, S., Mayo, K.E., Bell, G.I., 1992. Glucose transporter expression in brain. cDNA sequence of mouse GLUT3, the brain facilitative glucose transporter isoform, and identification of sites of expression by in situ hybridization. *J. Biol. Chem.* 267, 467–472.
- Nicholls, D.G., Ward, M.W., 2000. Mitochondrial membrane potential and neuronal glutamate excitotoxicity: mortality and millivolts. *Trends Neurosci.* 23, 166–174.
- Paolisso, G., Sgambato, S., Passariello, N., Giugliano, D., Scheen, A., D'Onofrio, F., Lefebvre, P.J., 1986. Insulin induces opposite changes in plasma and erythrocyte magnesium concentrations in normal man. *Diabetologia* 29, 644–647.
- Pauling, L., 1970. Evolution and the need for ascorbic acid. *Proc. Natl. Acad. Sci. U. S. A.* 67, 1643–1648.
- Ramadan, N.M., Halvorson, H., Vande-Linde, A., Levine, S.R., Helpert, J.A., Welch, K.M., 1989. Low brain magnesium in migraine. *Headache* 29, 590–593.
- Reiber, H., Ruff, M., Uhr, M., 1993. Ascorbate concentration in human cerebrospinal fluid (CSF) and serum. Intrathecal accumulation and CSF flow rate. *Clin. Chim. Acta* 217, 163–173.
- Ridha, B.H., Barnes, J., Bartlett, J.W., Godbolt, A., Pepple, T., Rossor, M.N., Fox, N.C., 2006. Tracking atrophy progression in familial Alzheimer's disease: a serial MRI study. *Lancet Neurol.* 5, 828–834.
- Rumsey, S.C., Kwon, O., Xu, G.W., Burant, C.F., Simpson, I., Levine, M., 1997. Glucose transporter isoforms GLUT1 and GLUT3 transport dehydroascorbic acid. *J. Biol. Chem.* 272, 18982–18989.
- Rumsey, S.C., Welch, R.W., Garraffo, H.M., Ge, P., Lu, S.F., Crossman, A.T., Kirk, K.L., Levine, M., 1999. Specificity of ascorbate analogs for ascorbate transport. Synthesis and detection of [(125)I]6-deoxy-6-iodo-L-ascorbic acid and characterization of its ascorbate-specific transport properties. *J. Biol. Chem.* 274, 23215–23222.
- Ryan, T.A., Reuter, H., Wendland, B., Schweizer, F.E., Tsien, R.W., Smith, S.J., 1993. The kinetics of synaptic vesicle recycling measured at single presynaptic boutons. *Neuron* 11, 713–724.
- Savini, I., Rossi, A., Pierro, C., Avigliano, L., Catani, M.V., 2008. SVCT1 and SVCT2: key proteins for vitamin C uptake. *Amino Acids* 34, 347–355.
- Schenk, J.O., Miller, E., Gaddis, R., Adams, R.N., 1982. Homeostatic control of ascorbate concentration in CNS extracellular fluid. *Brain Res.* 253, 353–356.
- Selkoe, D.J., 2002. Alzheimer's disease is a synaptic failure. *Science* 298, 789–791.
- Shcheglovitov, A., Shcheglovitova, O., Yazawa, M., Portmann, T., Shu, R., Sebastiano, V., Krawisz, A., Froehlich, W., Bernstein, J.A., Hallmayer, J.F., Dalmatsch, R.E., 2013. SHANK3 and IGF1 restore synaptic deficits in neurons from 22q13 deletion syndrome patients. *Nature* 503, 267–271.

- Shi, Z., Jiao, J., 2012. Direct lineage conversion: induced neuronal cells and induced neural stem cells. *Protein Cell* 3, 826–833.
- Shindo, Y., Fujimoto, A., Hotta, K., Suzuki, K., Oka, K., 2010. Glutamate-induced calcium increase mediates magnesium release from mitochondria in rat hippocampal neurons. *J. Neurosci. Res.* 88, 3125–3132.
- Siew, L.K., Love, S., Dawbarn, D., Wilcock, G.K., Allen, S.J., 2004. Measurement of pre- and post-synaptic proteins in cerebral cortex: effects of post-mortem delay. *J. Neurosci. Methods* 139, 153–159.
- Simpson, I.A., Vannucci, S.J., DeJoseph, M.R., Hawkins, R.A., 2001. Glucose transporter asymmetries in the bovine blood-brain barrier. *J. Biol. Chem.* 276, 12725–12729.
- Slutsky, I., Abumaria, N., Wu, L.J., Huang, C., Zhang, L., Li, B., Zhao, X., Govindarajan, A., Zhao, M.G., Zhuo, M., Tonegawa, S., Liu, G., 2010. Enhancement of learning and memory by elevating brain magnesium. *Neuron* 65, 165–177.
- Slutsky, I., Sadeghpour, S., Li, B., Liu, G., 2004. Enhancement of synaptic plasticity through chronically reduced Ca²⁺ flux during uncorrelated activity. *Neuron* 44, 835–849.
- Smiley, S.T., Reers, M., Mottola-Hartshorn, C., Lin, M., Chen, A., Smith, T.W., Steele Jr., G.D., Chen, L.B., 1991. Intracellular heterogeneity in mitochondrial membrane potentials revealed by a J-aggregate-forming lipophilic cation JC-1. *Proc. Natl. Acad. Sci. U. S. A.* 88, 3671–3675.
- Steffens, A.B., Scheurink, A.J., Porte Jr., D., Woods, S.C., 1988. Penetration of peripheral glucose and insulin into cerebrospinal fluid in rats. *Am. J. Physiol.* 255, R200–R204.
- Subramanian, A., Gupta, A., Saxena, S., Gupta, A., Kumar, R., Nigam, A., Kumar, R., Mandal, S.K., Roy, R., 2005. Proton MR CSF analysis and a new software as predictors for the differentiation of meningitis in children. *NMR Biomed.* 18, 213–225.
- Szelechowski, M., Betourne, A., Monnet, Y., Ferre, C.A., Thouard, A., Foret, C., Peyrin, J.M., Hunot, S., Gonzalez-Dunia, D., 2014. A viral peptide that targets mitochondria protects against neuronal degeneration in models of Parkinson's disease. *Nat. Commun.* 5, 5181.
- Tang, Y.P., Shimizu, E., Dube, G.R., Rampon, C., Kerchner, G.A., Zhuo, M., Liu, G., Tsien, J.Z., 1999. Genetic enhancement of learning and memory in mice. *Nature* 401, 63–69.
- Tarsa, L., Goda, Y., 2002. Synaptophysin regulates activity-dependent synapse formation in cultured hippocampal neurons. *Proc. Natl. Acad. Sci. U. S. A.* 99, 1012–1016.
- Terry, R.D., Masliah, E., Salmon, D.P., Butters, N., DeTeresa, R., Hill, R., Hansen, L.A., Katzman, R., 1991. Physical basis of cognitive alterations in Alzheimer's disease: synapse loss is the major correlate of cognitive impairment. *Ann. Neurol.* 30, 572–580.
- Thompson, J.A., Markey, S.P., Fennessey, P.V., 1975. Gas-chromatographic/mass-spectrometric identification and quantitation of tetrone and deoxytetrone acids in urine from normal adults and neonates. *Clin. Chem.* 21, 1892–1898.
- Thornalley, P.J., 1998. Glutathione-dependent detoxification of alpha-oxoaldehydes by the glyoxalase system: involvement in disease mechanisms and anti-proliferative activity of glyoxalase I inhibitors. *Chem. Biol. Interact.* 111–112, 137–151.
- Tsukaguchi, H., Tokui, T., Mackenzie, B., Berger, U.V., Chen, X.Z., Wang, Y., Brubaker, R.F., Hediger, M.A., 1999. A family of mammalian Na⁺-dependent L-ascorbic acid transporters. *Nature* 399, 70–75.
- Vannucci, S.J., Maher, F., Simpson, I.A., 1997. Glucose transporter proteins in brain: delivery of glucose to neurons and glia. *Glia* 21, 2–21.
- Wang, H., Hu, P., Jiang, J., 2013. Calcium bioavailability of calcium L-threonate in healthy Chinese subjects measured with stable isotopes ((⁴)(⁴)Ca and (⁴)(²)Ca). *Eur. J. Clin. Pharmacol.* 69, 1121–1126.
- Wang, H., Jiang, J., Hu, P., 2006. Determination of L-threonate in human plasma and urine by high performance liquid chromatography-tandem mass spectrometry. *J. Chromatogr. B Anal. Technol. Biomed. Life Sci.* 834, 155–162.
- Wang, H.Y., Hu, P., Jiang, J., 2011. Pharmacokinetics and safety of calcium L-threonate in healthy volunteers after single and multiple oral administrations. *Acta Pharmacol. Sin.* 32, 1555–1560.
- Yeh, W.L., Lin, C.J., Fu, W.M., 2008. Enhancement of glucose transporter expression of brain endothelial cells by vascular endothelial growth factor derived from glioma exposed to hypoxia. *Mol. Pharmacol.* 73, 170–177.
- Yu, N., Martin, J.L., Stella, N., Magistretti, P.J., 1993. Arachidonic acid stimulates glucose uptake in cerebral cortical astrocytes. *Proc. Natl. Acad. Sci. U. S. A.* 90, 4042–4046.
- Zhou, H., Liu, G., 2015. Regulation of density of functional presynaptic terminals by local energy supply. *Mol. Brain* 8, 42.